An Experimental Investigation into Active Structural Acoustic Cloaking of a Flexible Cylinder

Charlie House[a], Jordan Cheer[a] and Steve Daley[a]

[a]*Institute of Sound & Vibration Research, University of Southampton, University Road, Southampton, SO17 1BJ*

ARTICLE INFO

ABSTRACT

The ability to acoustically cloak an object, effectively making the object acoustically invisible to an outside observer, is of interest in many applications where the presence of an object has an undesirable impact on the sound-field. If a suitable disturbance signal can be measured, an active control system can be used to directly minimise the scattered acoustic pressure, which fully characterises the presence of the body. In this paper, a broadband feedforward active control system is used to minimise the scattered acoustic pressure at a far-field microphone array using an array of structural control sources affixed to the flexible scattering body. The performance of this system is assessed using measured data corresponding to a hollow cylindrical shell subject to an incident acoustic field, and the causality of the control filters is investigated. It is shown that the practical causality constraint limits the performance of the active cloak at lower frequencies, but the causally constrained controller is able to achieve approximately 10 dB of attenuation in the far-field scattered acoustic power, using an array of 9 control actuators. The influence that the number of control actuators has on the attenuation performance is investigated, the practicability of the system is discussed, and a number of potential implementation challenges are identified, including the increased level of structural vibration caused by the active structural acoustic cloaking system.

1. Introduction

Acoustic cloaking has been a topic of significant research interest for an extended period of time as the ability to render an object acoustically invisible, such that the sound-field with the object present is identical to that without the object present, has benefits in both research and engineering applications. For example, there is an interest in acoustic cloaking to attenuate the self-scattering effects from Unmanned Underwater Vehicles (UUVs) when performing subsurface acoustic measurements [1, 2]. Alternatively, there is an interest in reducing the acoustic scattering from architectural features in performance spaces, which can cause unwanted early-reflections [3] that reduce intelligibility and clarity for an audience [4].

The general principle of acoustic cloaking can be achieved either passively, where the object is cloaked using an acoustic metamaterial [5, 6, 7, 8, 9], or actively, where destructive interference and secondary control sources are used to attenuate the scattered field [10, 11, 12, 13, 14]. Both methods have their respective advantages and disadvantages. For example, passive acoustic cloaking is relatively low-cost, since it requires no actuators, sensors, or Digital Signal Processing (DSP) and, therefore, no electrical power supply. However, passive acoustic cloaks generally have a relatively narrow bandwidth of operation and are not straightforward to reconfigure for different situations [15, 16]. Active acoustic cloaking methods, conversely, rely on the availability of costly active components including actuators, sensors and DSP, but can potentially operate over relatively wide bandwidths [17]

and, as with active systems in general [18], can inherently be designed to adapt to changes in the environment. This study will focus on an experimental implementation of an active structural acoustic cloaking system.

The theoretical basis of active noise and vibration control is well established [18, 19, 20] and over the past 3 decades or so, a broad variety of engineering noise and vibration control problems have been solved using active control technologies. A large number of practical active noise control systems make use of Active Structural Acoustic Control (ASAC), where structural actuation is used to minimise the noise radiated from, or transmitted through, a structure [20, 21, 22, 23, 24]. By directly controlling the structure, a global reduction in radiated sound power can be achieved with a lower number of control sources than with conventional active noise control. When combined with a remote sensing strategy, ASAC has the advantage that the entire control system can be contained within the structure, without the requirement for far-field transducers [25, 26, 27].

Whilst a wide range of practical active control systems have been presented in the literature, active acoustic cloaking remains a challenging area of practical research interest. Although there have been many theoretical and simulation based investigations into active acoustic cloaking [17, 28], practical studies are more limited, as these methods all assume real-time knowledge of the scattered acoustic pressure. In practice, the scattered pressure cannot be measured directly and any acoustic sensor will measure the superposition of the incident and scattered components of the sound-field [29]. This means that the scattered pressure must first be estimated before being utilised as the error signal in an active control system. This estimation can potentially be achieved

in a number of ways, including the use of a Virtual Sensing strategy [30], by using analytical or numerical modelling [31], or by using a wave decomposition approach [10].

An alternative active acoustic cloaking method uses control sources to cancel out the incident pressure in the near-field of the scattering object, effectively generating a quiet-zone around the scatterer so that the incident field does not reach the scattering body, whilst also enforcing a constraint on the exterior radiation from the control sources so that the far-field sound-field is unaffected. As the incident pressure is reduced around the object, the back-scattered pressure is also reduced without the controller needing any knowledge of the scattering object or an estimation of the scattered pressure. The potential performance of this approach has been predicted analytically [11, 12, 13, 32], however, these studies have generally assumed that either high order multipole control sources are available, or that a continuous distribution of monopole and dipole sources can be used. In practice, neither of these arrangements are practicable and, therefore, no experimental validations of this approach have been published to-date.

When using a discrete number of active sources to attenuate an exterior pressure-field, as is the case in active acoustic cloaking, Huygen's principle dictates that these control sources should be as close as possible to the primary source [19, 33]. In the case of active acoustic cloaking, this has been investigated via a simulation-based study in [17], and it has been shown that the control sources should be located as close as possible to the scattering object, which acts as the primary source of the scattered acoustic field. For a practical active acoustic cloaking system utilising acoustic control sources, the minimum distance between the scattering object and the control sources is defined by the physical size of the control sources. This practical constraint potentially limits the performance of an active acoustic cloaking system using acoustic control sources, however, it can be overcome if structural control sources are used, as proposed previously by [14, 34, 35, 36]. As noted by Eggler et al [14], this can be directly compared to the Active Structural Acoustic Control systems discussed above [20, 21, 22, 23, 24], and Eggler et al [14] consequently labelled this approach Active Structural Acoustic Cloaking.

Eggler et al [14] used analytical simulations to investigate the difference in the active acoustic cloaking performance that can be achieved when using either acoustic or structural control sources. This work demonstrated that for an infinite elastic cylinder, structural point forces are able to achieve higher levels of attenuation in the scattered acoustic field than when using acoustic monopole control sources. The current paper will extend the simulation-based study reported by Eggler et al [14], by presenting an experimental investigation into active structural acoustic cloaking. Eggler et al [14] showed physical insight into the controllability problem, which will be developed in the current study by investi-

gating how the performance is limited when a practical reference signal is utilised for non-tonal acoustic disturbances, and the effect of applying the cloaking strategy to a finite-sized structure. In particular, a practical method of obtaining a reference signal is proposed, which is based on an Internal Model Control architecture, and the effects of causally constraining the control filters are explored, as this is required for the control of broadband signals in practice. Additionally, the influence of the active acoustic cloaking strategy on the structural response is investigated for the first time and the requirements in terms of the number of control actuators are also investigated for a finite sized structure.

An overview and discussion of previous work has been presented in Section 1. Section 2 will present details of the scattering object, the experimental setup, and the procedure used to measure the scattered acoustic pressure. Section 3 will outline the active structural acoustic cloaking strategy and formulate optimal control filters both with and without a constraint on the causality. Section 4 will present an investigation into the limits on the performance of the active structural acoustic cloaking strategy using the measured responses. Finally, conclusions, and a brief discussion of the real-world practicalities of the proposed control system will be presented in Section 5.

2. Experimental Setup

In order to investigate the practical limits on active structural acoustic cloaking, a series of both structural and acoustic measurements have been carried out in the Large Anechoic Chamber at the Institute of Sound & Vibration Research and details of these measurements are described in this section. As shown in Figure 1, the scattering body utilised during this study consisted of a hollow aluminium cylindrical shell of length 1.4 m, radius 0.23 m and wall thickness 6.4 mm, which was suspended inside the anechoic chamber on a pair of flexible mounts.

When designing a control system it is important to ensure that the disturbance to be reduced is both controllable and observable [37]. That is, the error sensors should be located such that they are able to fully characterise the disturbance to be controlled, and the control sources should be located such that they are able to reduce the unwanted disturbance. For the system discussed in this paper, this requires the control sources to be arranged on the cylinder such that, within the given frequency range, they do not all fall into nodal regions of the cylinder's mode shapes. To ensure that this is the case, a set of structural identification measurements were first carried out to characterise the modal response of the cylinder. Experimentally, an array of 96 accelerometers was mounted to the body of the cylinder, arranged in lines of 12 running axially along the length of the cylinder, each measuring the radial component of the structural acceleration when the cylinder was excited acoustically by a far-field source driven by white noise that was band-
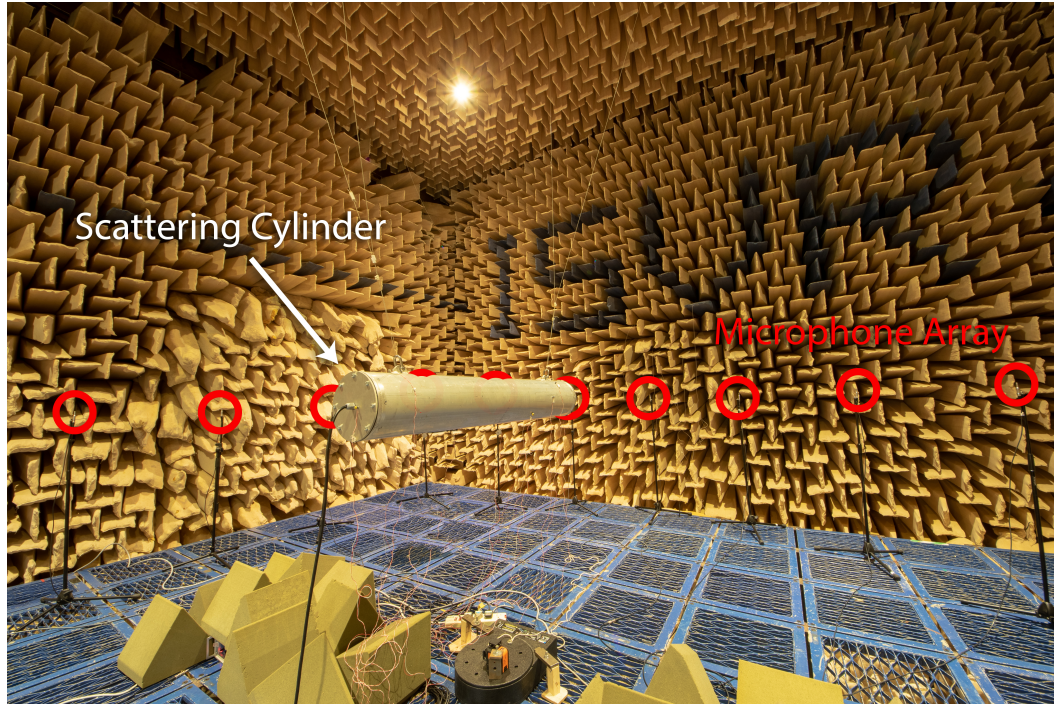
Figure 1: Photograph of the experimental setup, showing the cylinder and far-field microphones. The cylinder and the far-field microphone array are labelled.

limited between 100 and 1000 Hz. The resulting transfer responses between the acoustic source and each structural measurement on the cylinder were then used to identify the four dominant structural resonances within the considered bandwidth. These experimentally identified operational deflection shapes are plotted in Figure 2, along with the corresponding resonant frequencies. For comparison, a numerical modal analysis of the finite cylinder was also carried out and the resulting mode shapes and modal frequencies are also presented in Figure 2. It can be seen from Figure 2 that there is a strong correlation between the numerical and experimental results, with both datasets showing consistent deflection shapes for the four dominant resonances below 1 kHz. Knowledge of these will direct the placement of structural actuators and accelerometers throughout the rest of the experimental procedure.

To enable an investigation into the practical limits of an active structural acoustic cloaking system and to investigate its effect on the structural response, it is necessary to instrument the scattering cylinder with control actuators and structural sensors, and to use an array of microphones to measure the acoustic field. Based on the modal analysis discussed above, an array of structural actuators (Tectonic Elements TEAX32C30) was attached to the inside of the cylindrical shell to provide control actuation, as shown in Figure 3. To ensure that the control actuators were able to couple into the dominant structural modes, as shown in Figure 2, the actuators were arranged in three rings of three actuators, with a 120° separation between the actuators in each ring and an offset of 60° between consecutive rings along the length of

the cylinder, as shown in Figure 3. As can also be seen in Figure 3, the actuators were oriented to apply a force in the radial direction. To monitor the response of the structure and thus provide new insight into the effect of active structural acoustic cloaking on the structural vibration, an array of 12 accelerometers (PCB A352 / C67) was also mounted to the cylinder, arranged in a spiral along its length in order to sufficiently detect the contribution from all of the dominant resonances shown in Figure 2, with each accelerometer measuring the radial response, as shown in Figure 4. To measure both the incident and scattered sound fields, as well as the sound field generated by driving the structural control actuators, a far-field microphone array, consisting of 20 microphones (PCB 130F20), was arranged in a circle of radius 2.8 m surrounding the scattering cylinder, as shown in Figure 5. Finally, the incident pressure field was generated by a primary disturbance that was provided by a dual-concentric high-powered loudspeaker (Tannoy CPA12), placed outside of the microphone array, oriented towards the midpoint of the cylinder, as also shown in Figure 5.

The experimental setup shown in Figure 5 has been used to obtain the acoustic and structural transfer responses, which will subsequently be used to investigate the performance of active structural acoustic cloaking. Transfer responses between each source (1 primary acoustic source and 9 structural control sources) and each structural and acoustic sensor have been measured with the cylinder present in the anechoic chamber. Under this condition, the responses measured at each microphone when the primary source is driven give the vector of total acoustic pressures, $\mathbf{d}_t$, which can be expressed
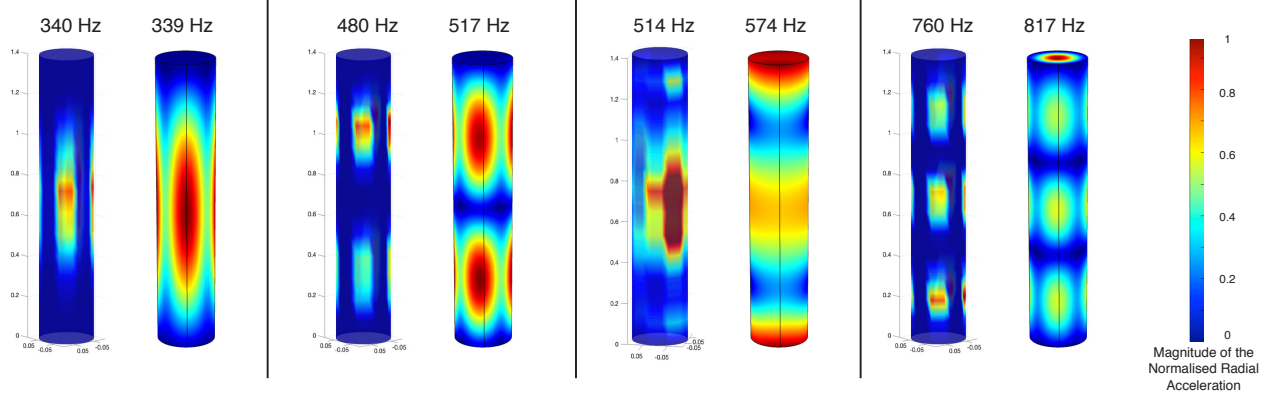
Figure 2: The operational deflection shapes, mode shapes and resonant frequencies of the four dominant structural resonances of the cylinder below 1kHz. The left-hand plot in each case shows the measured data and the right-hand plot shows the corresponding results calculated using a numerical model.
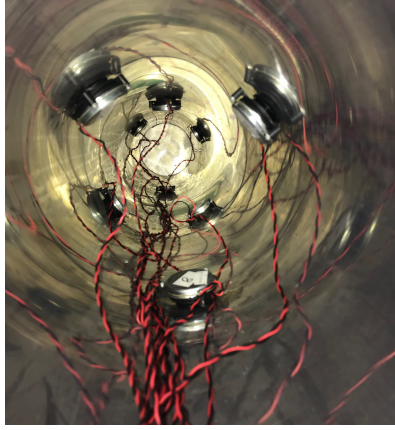

Figure 3: Photograph looking down the length of the inside of the cylinder, showing the locations of the control actuators.
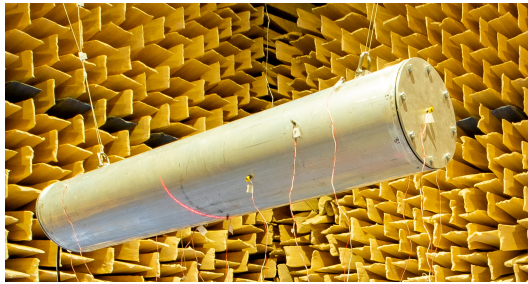

Figure 4: Photograph of the experimental setup, showing the accelerometers mounted to the cylinder.

Figure 5: Diagram of the experimental layout, showing the scattering cylinder, far-field pressure microphones, structural actuators and primary disturbance location.

in terms of the linear summation of the vector of incident, $\mathbf{d}_i$, and scattered, $\mathbf{d}_s$, pressures as

$$\mathbf{d}_t = \mathbf{d}_i + \mathbf{d}_s. \tag{1}$$

It should be highlighted that the scattered pressure, $\mathbf{d}_s$, includes the components due to both the rigid body and flexible body scattering and thus fully characterises the effect of the flexible scattering body. To extract the scattered pres-
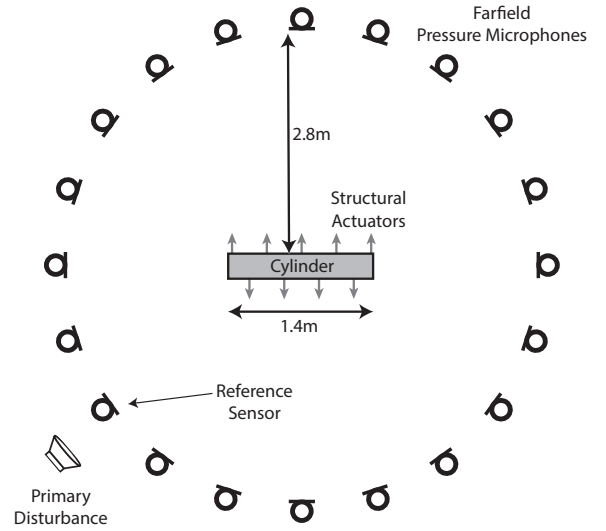
sures from these measurements, it is necessary to remove the cylinder and measure the transfer responses between the primary source and the array of microphones, which provides a direct measure of the incident pressures at each microphone location, $\mathbf{d}_i$. According to Equation 1, the scattered acoustic pressure can then be calculated at each microphone location by subtracting the vector of incident pressures, $\mathbf{d}_i$, from the vector total pressures, $\mathbf{d}_t$. Although this method provides a measure of the scattered acoustic field that can be utilised to implement an active acoustic cloaking system in a stationary sound field, it is clearly not a practical solution for the implementation of a real-time controller in the
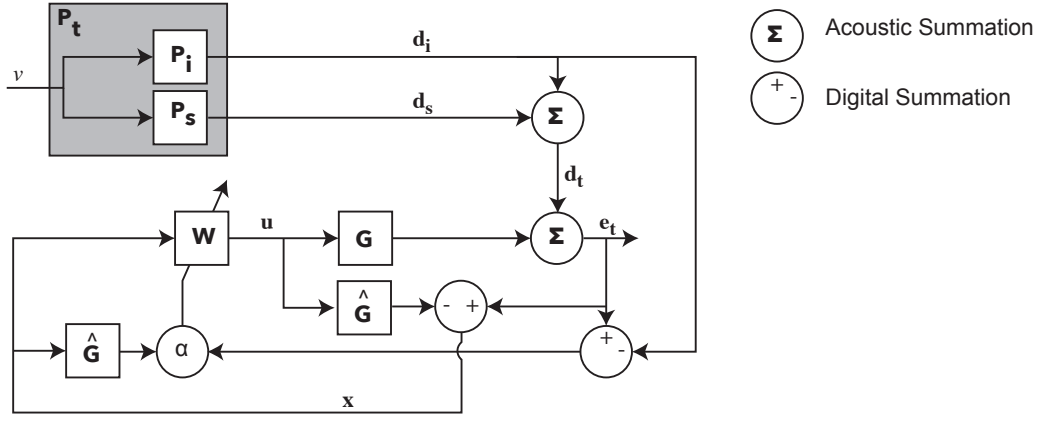
Figure 6: Block diagram showing the formulation of the Internal Model Control (IMC) Filtered-Reference Least Mean Squares (FxLMS) active control system.

presence of changes in the primary disturbance or the acoustic environment. Although a number of previous publications have investigated methods of estimating the scattered acoustic field in real-time [10, 38, 31, 30], these also rely on knowledge of the acoustic field with and without the scattering body present. This means that these strategies cannot yet be readily applied to practical active cloaking strategies where the acoustic environment is non-stationary. It is also pertinent to note that in the case of [10, 38], response measurements between the control sources and error sensors both with and without the scattering body present are used and, in the case of active structural acoustic cloaking, such measurements would not be possible, as removing the scattering body would also remove the control sources. Based on these limitations, it is clear that further work is required in this area to allow real-time estimation of the scattered acoustic field in non-stationary environments. However, the present paper focuses on the effectiveness of structural actuation as a control mechanism for active acoustic cloaking and the limitations imposed by a practical causally constrained controller and, therefore, insight can be provided into the control strategy without overcoming the limitations in terms of scattered field detection.

3. Broadband Control Formulations

This section describes the feedforward control strategy used to implement an active structural acoustic cloaking system. The block diagram showing the architecture of the controller is presented in Figure 6, from which it can be seen that the adopted strategy is a feedforward filtered reference system, with an Internal Model Control (IMC) architecture providing the reference signal. In order to understand the limits on the control performance, the optimal broadband control filters will be used, derived in this section both with and without causality constraints and these optimal filters will be utilised in Section 4 in conjunction with the measured transfer responses, as discussed in the previous section.

Following the discussion presented in Section 2, the vector of total acoustic pressures, at a single frequency, at the array of L error microphones before control, $\mathbf{d}_t\left(e^{j\omega}\right)$, can be expressed by the summation of the vectors of incident pressures and scattered pressures at the error microphones which, at a single frequency, gives

$$\mathbf{d}_t\left(e^{j\omega}\right) = \mathbf{d}_i\left(e^{j\omega}\right) + \mathbf{d}_s\left(e^{j\omega}\right), \qquad (2)$$

where $\mathbf{d}_t$ is the vector of total pressures, $\mathbf{d}_i$ is the vector of incident pressures, $\mathbf{d}_s$ is the vector of scattered pressures, ω is the angular frequency and j is a unit imaginary number. For clarity of expression, the frequency dependence will be dropped in the subsequent formulations. As shown in Figure 6, the total pressure at the error microphones after control, $\mathbf{e}_t$, is given by the linear superposition of the total disturbance, $\mathbf{d}_t$, and the pressures at the error microphones due to control, which gives

$$\mathbf{e}_t = \mathbf{d}_t + \mathbf{G}\mathbf{u}, \qquad (3)$$

where $\mathbf{u}$ is the vector of control signals and $\mathbf{G}$ is the matrix of complex transfer responses between the control sources and the error microphones, which is generally referred to as the plant response in the context of active control [18, 19, 20]. As shown in Figure 6, the control signals are calculated by filtering the reference signal, $\mathbf{x}$, via the matrix of control filters, $\mathbf{W}$, which gives

$$\mathbf{u} = \mathbf{W}\mathbf{x}. \qquad (4)$$

The choice of reference signals is critical to the operation of active noise control systems and, in general, the reference signal should be coherent with the error signals and provide some time-advance for the control system to operate. In the case of active cloaking, the primary source generating the incident pressure field is usually unknown and, therefore, cannot be accessed to provide a reference signal. However, as discussed in the introduction, the scattered field, which

forms the error signals to be cancelled, is effectively generated by the scattering object. Therefore, it may be possible to position the reference sensors in close proximity to the scattering body to provide some time advance between the reference signals and the outgoing scattered field. In the present study, a single layer of error microphones are employed, as shown in Figures 1 and 5, and, therefore, an IMC architecture will be utilised [39] along with a Filtered-reference Least Mean Squares (FxLMS) adaptive algorithm. Using this control architecture, the reference signals are provided by estimates of the disturbance signals at the error microphones. Although this may somewhat limit the time-advance between the reference and error signals, it provides a highly coherent reference signal and has been shown to be an effective strategy in a variety of practical applications [40, 41]. An estimate of the vector of total pressures at the error microphones before control, $\hat{\mathbf{d}}_t$, can be calculated as shown in Figure 6 by compensating for the control source contributions at the error microphones, which gives

$$\hat{\mathbf{d}}_t = \mathbf{e}_t - \hat{\mathbf{G}}\mathbf{u}, \qquad (5)$$

where $\hat{\mathbf{G}}$ is an estimate of the plant response.

In the context of active acoustic cloaking, the aim of the controller is to generate a control field such that the sound field after control is equal to the incident sound field, thus cloaking the scattering body. By substituting Equation 2 into Equation 3, it can be seen that the total pressure at the error sensors after control is given by

$$\mathbf{e}_t = \mathbf{d}_i + \mathbf{d}_s + \mathbf{G}\mathbf{u}. \qquad (6)$$

Therefore, by cancelling the scattered pressures using the control sources, the total pressure after control becomes equal to the incident field and the scattering body will be effectively cloaked. Minimisation of the scattered acoustic field can be expressed in terms of the space-averaged mean square scattered pressure in the far-field, which can be approximated by the cost function defined as

$$J = \mathrm{E}\left[\mathbf{e}_s^H \mathbf{e}_s\right], \qquad (7)$$

where E is the expectation operator and $\mathbf{e}_s$ is scattered acoustic pressure at the error sensors after control, which can be expressed as

$$\mathbf{e}_s = \mathbf{d}_s + \mathbf{G}\mathbf{u}. \qquad (8)$$

As shown in Figure 6, it is assumed that this is calculated from the directly measured error signals, $\mathbf{e}_t$, as

$$\mathbf{e}_s = \mathbf{e}_t - \mathbf{d}_i, \qquad (9)$$

where the incident disturbance signals have been identified a priori. In practice, as discussed in Section 2, it may be possible to estimate the incident field using a variety of methods, such as wave decomposition or virtual sensing, but these methods are still limited in the context of non-stationary environments and, therefore, future work is required in this

area before practical real-time active cloaking systems can be realised.

In the following two sections, the optimal control filters will be calculated that minimise the cost function defined in Equation 7, firstly with no constraint on the causality and subsequently when a causality constraint is introduced. The full multi-channel formulations will be presented, which assume that M control sources are used to minimise the scattered pressures at L error sensors, using K reference signals, and a control filter with a tap-length of I samples.

3.1. Causally Unconstrained Optimal Controller

The causally unconstrained controller can be derived in the frequency domain and can be calculated at each frequency bin independently to build up the full broadband performance. Firstly, combining Equations 4, 7 and 8 gives the cost function to be minimised in Hermitian quadratic form as

$$J = \mathrm{trace}\left[\mathrm{E}\left[\mathbf{GWxx}^H\mathbf{W}^H\mathbf{G}^H + \mathbf{GWxd}_s^H + \mathbf{d}_s\mathbf{x}^H\mathbf{W}^H\mathbf{G}^H + \mathbf{d}_s\mathbf{d}_s^H\right]\right]. \qquad (10)$$

By defining the matrices of power and cross spectral densities between the reference and disturbance signals as

$$\mathbf{S}_{xx} = \mathrm{E}\left[\mathbf{xx}^H\right], \qquad (11)$$

$$\mathbf{S}_{xd} = \mathrm{E}\left[\mathbf{d}_s\mathbf{x}^H\right], \qquad (12)$$

$$\mathbf{S}_{dd} = \mathrm{E}\left[\mathbf{d}_s\mathbf{d}_s^H\right], \qquad (13)$$

the cost function can be simplified to give

$$J = \mathrm{trace}\left[\mathbf{GWS}_{xx}\mathbf{W}^H\mathbf{G}^H + \mathbf{GWS}_{xd}^H + \mathbf{S}_{xd}\mathbf{W}^H\mathbf{G}^H + \mathbf{S}_{dd}\right]. \qquad (14)$$

By differentiating Equation 14 with respect to the real and imaginary parts of the matrix of control filter coefficients, and setting the result to zero as detailed in [18], the matrix of optimal control filters is given as

$$\mathbf{W}_{\mathbf{opt}} = -\left[\mathbf{G}^H\mathbf{G} + \beta\mathbf{I}\right]^{-1}\mathbf{G}^H\mathbf{S}_{xd}\mathbf{S}_{xx}^{-1}, \qquad (15)$$

where $\mathbf{I}$ is an identity matrix, and it is assumed that both $\mathbf{G}^H\mathbf{G}$ and $\mathbf{S}_{xx}$ are invertible. To constrain the control effort, and to reduce the effect of poor conditioning on the matrix inversion, Tikhonov regularisation [42] has been included and can be adjusted with the regularisation parameter β.

3.2. Causally Constrained Optimal Controller

In practice, it is necessary to constrain the broadband control filters to be causal and the optimal broadband filter responses in this case can be derived in the time-domain, as in [18] for the standard feedforward active noise control system. To this end, the scattered acoustic pressure measured at the l-th error microphone after control can be expressed at the n-th time step as

$$e_{s_l}(n) = d_{s_l}(n) + \sum_{m=1}^{M}\sum_{j=0}^{J-1}\sum_{k=1}^{K}\sum_{i=0}^{I-1} g_{lmj}w_{mki}x_k(n-i-j), \qquad (16)$$

where $d_{s_l}(n)$ is the scattered pressure at the l-th error sensor due to the primary disturbance, g_{lmj} is the j-th coefficient of the J-th order FIR filter approximating the plant response between the m-th control source and the l-th error sensor, w_{mki} is the i-th coefficient of the I-th order FIR control filter corresponding to the m-th control source and the k-th reference signal, and x_k is the k-th reference signal. By assuming the controller is time invariant, Equation 16 can be rewritten as

$$e_{s_l}(n) = d_{s_l}(n) + \sum_{m=1}^{M} \sum_{k=1}^{K} \sum_{i=0}^{I-1} w_{mki} r_{lmk}(n-i), \quad (17)$$

where r_{lmk} is the k-th reference signal filtered by the plant response between the m-th control source and the l-th error microphone. The filtered reference signal can be expressed as

$$r_{lmk}(n) = \sum_{j=0}^{J-1} g_{lmj} x_k(n-j). \quad (18)$$

For convenience, Equation 17 can be expressed in vector form as

$$e_{s_l}(n) = d_{s_l}(n) + \sum_{i=0}^{l-1} \mathbf{w}_i^{\mathrm{T}} \mathbf{r}_l(n-i), \quad (19)$$

where $\mathbf{w}_i$ and $\mathbf{r}_l(n)$ are defined as

$$\mathbf{w}_i = \left[w_{11i}, w_{12i}, \ldots, w_{1Ki}, w_{21i}, \ldots w_{MKi} \right]^{\mathrm{T}} \quad (20)$$

$$\mathbf{r}_l(n) = \left[r_{l11}(n), r_{l12}(n), \ldots \right.$$
$$\left. , r_{l1K}(n), r_{l21}(n), \ldots, r_{lMK}(n) \right]^{\mathrm{T}}. \quad (21)$$

The multichannel control problem can then be formulated by expressing the vector of L error signals in the time domain as

$$\mathbf{e}_s(n) = \mathbf{d}_s(n) + \mathbf{R}(n)\mathbf{w}, \quad (22)$$

where

$$\mathbf{e}_s(n) = \left[e_{s_1}(n), \ldots, e_{s_L}(n) \right]^{\mathrm{T}}, \quad (23)$$

$$\mathbf{d}_s(n) = \left[d_{s_l}(n), \ldots, d_{s_l}(n) \right]^{\mathrm{T}}, \quad (24)$$

$$\mathbf{R}(n) = \begin{bmatrix} \mathbf{r}_1(n)^{\mathrm{T}} & \mathbf{r}_1(n-1)^{\mathrm{T}} & \ldots & \mathbf{r}_1(n-I+1)^{\mathrm{T}} \\ \mathbf{r}_2(n)^{\mathrm{T}} & \mathbf{r}_2(n-1)^{\mathrm{T}} & \ldots & \mathbf{r}_2(n-I+1)^{\mathrm{T}} \\ \vdots & \vdots & & \vdots \\ \mathbf{r}_L(n)^{\mathrm{T}} & \mathbf{r}_L(n-1)^{\mathrm{T}} & \ldots & \mathbf{r}_L(n-I+1)^{\mathrm{T}} \end{bmatrix}, \quad (25)$$

and the MKI vector of control filter coefficients is defined as

$$\mathbf{w} = \left[\mathbf{w}_0^{\mathrm{T}}, \mathbf{w}_1^{\mathrm{T}} \ldots \mathbf{w}_{I-1}^{\mathrm{T}} \right]. \quad (26)$$

As in the case of the causally unconstrained controller, the cost function is defined by Equation 7. Substituting Equation 22 into Equation 7 gives the quadratic cost function as

$$J = \mathbf{w}^{\mathrm{T}} \mathrm{E}\left[\mathbf{R}^{\mathrm{T}}(n)\mathbf{R}(n) \right] \mathbf{w} + 2\mathbf{w}^{\mathrm{T}} \mathrm{E}\left[\mathbf{R}^{\mathrm{T}}(n)\mathbf{d}_s(n) \right]$$
$$+ \mathrm{E}\left[\mathbf{d}_s^{\mathrm{T}}(n)\mathbf{d}_s(n) \right]. \quad (27)$$

Assuming that $\mathrm{E}\left[\mathbf{R}^{\mathrm{T}}(n)\mathbf{R}(n) \right]$ is positive definite, this cost function has a unique global minimum and the optimal set of control filters that minimises the scattered acoustic field at the error sensors is given as

$$\mathbf{w}_{opt} = -\left[\mathrm{E}\left[\mathbf{R}^{\mathrm{T}}(n)\mathbf{R}(n) + \beta \mathbf{I} \right] \right]^{-1} \mathrm{E}\left[\mathbf{R}^{\mathrm{T}}(n)\mathbf{d}_s(n) \right]. \quad (28)$$

As with the causally unconstrained solution given by Equation 15, Tikhonov regularisation has been included, which introduces a constraint on the control effort, via the regularisation parameter β.

4. Experimental Investigation of Active Structural Acoustic Cloaking Limitations

In the following analysis, the acoustic measurements described in Section 2 will be used to investigate the performance limitations of the feedforward control strategy presented in Section 3. As shown in Figure 5, the total pressure measured at the microphone directly in-front of the primary disturbance will be used to provide the reference signal, which will be calculated using the IMC structure shown in Figure 6 and described in Section 3. The FxLMS controller will be implemented using $M = 9$ control actuators to minimise the scattered acoustic pressure at $L = 20$ farfield microphones using a control filter of length $I = 512$ samples at a sampling frequency of $f_s = 2000$ Hz. The regularisation parameters in each case have been selected so as to ensure that the magnitude of the dominant peak in the control filter impulse responses are approximately equal between the causally constrained and causally unconstrained control filters.

4.1. Limits Due to Causality

In order to understand the limits on the performance of the active structural acoustic cloaking control system described in Section 2, this section will compare the performance of the causally constrained and unconstrained controllers in order to provide insight into the limits imposed by both enforcing causality and the proposed method of obtaining a time-advanced reference signal. The performance of the control systems can be evaluated in terms of the cost function defined in Equation 7 and, provided that the error microphones are positioned in the far-field, this can be related to the scattered acoustic power as [33]

$$W_s = \frac{J}{2\rho_0 c_0} \quad (29)$$

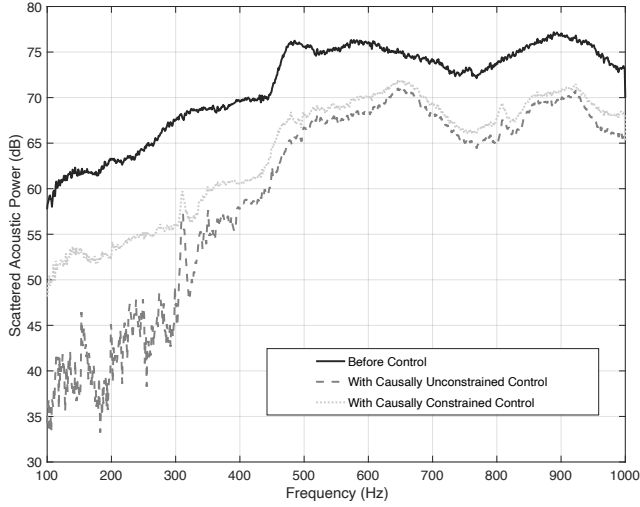where ρ_0 is the fluid density and c_0 is the speed of sound in the fluid.

Figure 7: The scattered acoustic power before control, with broadband unconstrained control, and with broadband causally constrained control.

Figure 8: The group delay between the reference signal and the scattered pressure error signal at the reference microphone, as shown in Figure 5.

The scattered acoustic power has been calculated for both the causally unconstrained and constrained controllers, and is presented in Figure 7, along with the scattered acoustic power before control. From these results it can be seen that the causally constrained controller is able to achieve between around 5 and 10 dB of attenuation across the presented bandwidth. By removing the constraint on the causality of the control filter, it can be seen that performance at frequencies below around 400 Hz is significantly increased, with an attenuation of around 20 dB at 100 Hz. At frequencies above approximately 500 Hz, however, the difference between the causally constrained and unconstrained controllers is only around 1 dB.

The difference in performance achieved between the causally constrained and unconstrained controllers can be explained by evaluating the time-advance provided by the reference signal. This can be evaluated in terms of the group delay [43] between the reference signal, calculated according to Equation 5, and the scattered pressure error signal at the same microphone position, given by Equation 8. The calculated group delay is shown in Figure 8 as a function of frequency and from these results it is shown that the proposed reference signal provides a time advance compared to the error signal of around 6 ms over the considered bandwidth. There is a slight increase in the group delay with frequency, but importantly, at lower frequencies the time advance is not much greater than the period of oscillation and this limits the achievable control performance at lower frequencies when causality is enforced, as shown in Figure 7. For reference, the impulse response of the control filter corresponding to the first actuator for the causally constrained and unconstrained control strategies is presented in Figure 9, and this shows the significant non-causal component in the unconstrained filters. The control filter responses for all 9 actuators are consistent in form to the examples presented in
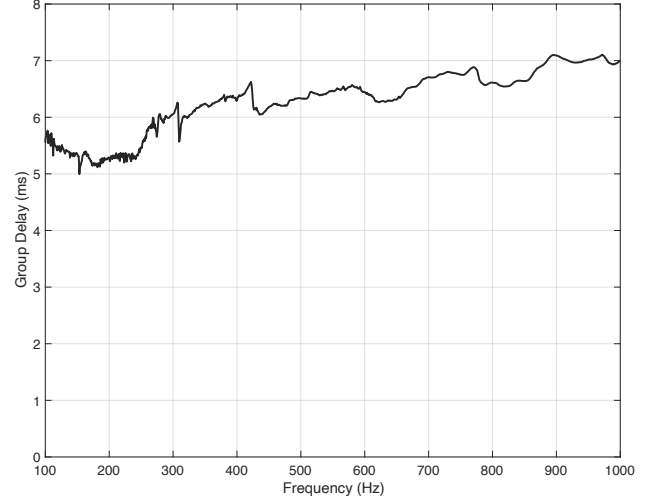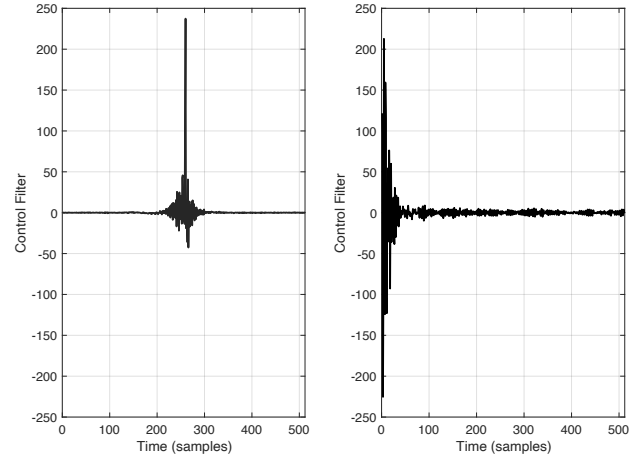

Figure 9: The impulse responses of the control filter for the first actuator, with both the causally unconstrained (left) and causally constrained (right) controllers.

Figure 9.

Whilst Figure 7 presents the performance of the two control algorithms over frequency, it is also insightful to observe how the control strategies affect the directivity of the acoustic scattered pressure. Figure 10 shows the directivity of the scattered pressure at the frequencies corresponding to each of the four dominant modes of the structure, as identified in Figure 2. The directivities of the scattered pressure are shown both before control, and after control using the causally constrained and unconstrained control strategies. For reference, the orientation of the cylinder has been marked on each plot in Figure 10 and the direction of propagation of the incident field is indicated by the arrow. The 480 Hz and 514 Hz plots in Figure 10 clearly show the two main lobes of the scattered pressure field, with the specular
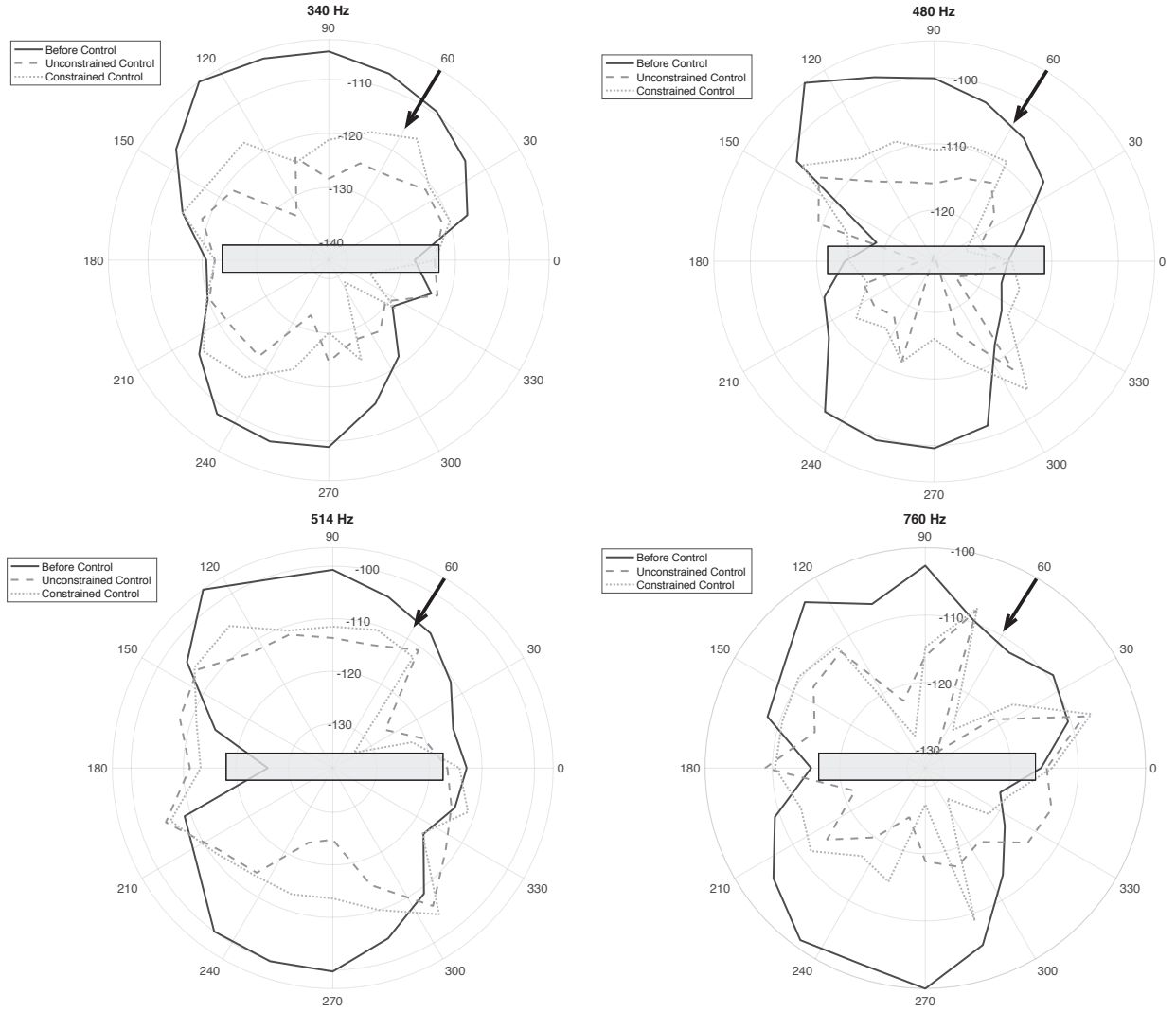
Figure 10: Polar plots showing the directivity of the scattered pressure field at the frequencies corresponding to the four dominant modes of the cylinder before control, with broadband unconstrained control, and with broadband causally constrained control. The direction of the incident wave is marked with an arrow.

reflection occurring in the 120° direction and the scattered field that results in acoustic shadowing being most prominent in the 240° direction. It is interesting to note that while the active structural acoustic cloaking strategies are effective at achieving significant reductions in the acoustic scattered power, as shown by the results presented in Figure 7, it is clear from the results in Figure 10 that both constrained and unconstrained controllers produce some enhancement in the acoustic scattered pressure in certain directions. In general, these enhancements occur in directions where the uncontrolled scattered field is low in level and, therefore, the controllers are effectively trading off the enhancement to achieve significant reductions in directions where the uncontrolled scattered field is dominant.

To provide more insight into the effects of constraining the causality of the control system, the control effort for each controller has been calculated as

$$\mathrm{CE} = 10 \log_{10} \left[\mathbf{u}^{\mathrm{H}} \mathbf{u} \right] . \tag{30}$$

The control effort provides an indication of the power required by a control system and the results for the causally constrained and unconstrained controllers are presented over frequency in Figure 11. These results show that the causally constrained controller requires significantly more energy at low frequencies, despite achieving a lower level of reduction in the scattered power. Above approximately 800 Hz, both the causally unconstrained and causally constrained controllers are almost identical in terms of both performance and control effort. It is worth noting that the performance of any practical system will be limited by the maximum force output of the control actuators, and it should be ensured that the required control effort is within the linear operating range of the actuators.
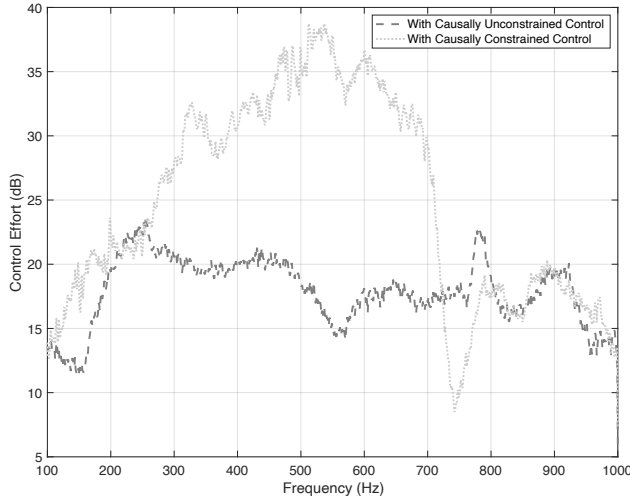
Figure 11: The control effort in decibels plotted against frequency for both the causally unconstrained and causally constrained controllers.

Figure 12: The structural response of the cylinder when it is excited by the incident acoustic field without control, and with both causally unconstrained control and causally constrained control.

4.2. Effect of Active Cloaking on the Structural Response

In addition to investigating the effect of active structural acoustic cloaking on the scattered acoustic field, it is also insightful and of practical interest to investigate how the structural response of the cylinder is affected by the active cloaking strategy. In certain applications, an active structural acoustic cloaking system that significantly increases the vibration of the structure would not be acceptable, even if it does not radiate, and therefore it may be necessary to constrain the levels of structural enhancement or adopt alternative control methods.

In addition to the array of structural actuators shown in Figure 3, an array of 12 accelerometers was also attached to the cylinder to measure the radial component of the cylinder vibration, as previously described in Section 2. Figure 12 shows the sum of the squared accelerometer signals when the cylinder is excited by the primary acoustic field, and when acoustic scattering is controlled using the two control formulations. Figure 12 clearly shows the four main structural resonances of the cylinder, corresponding to the dominant modes outlined in Figure 2. From these results it can be seen that both control strategies result in a significant increase in the structural vibration across the presented frequency range. This indicates that the structure is effectively being used as an acoustic radiator to achieve the acoustic control, as in the case of active structural acoustic control systems [21, 23, 24, 25, 27]. This result also indicates that rather than the active cloaking system driving the structure to behave as an acoustically rigid body, which scatters less on resonance than an elastic body [35, 44], the structure is being driven in a more complex manner to maximise the reduction in the scattered acoustic field. The differences between the causally constrained and causally unconstrained results shown in Figure 12 can be related to the correspond-
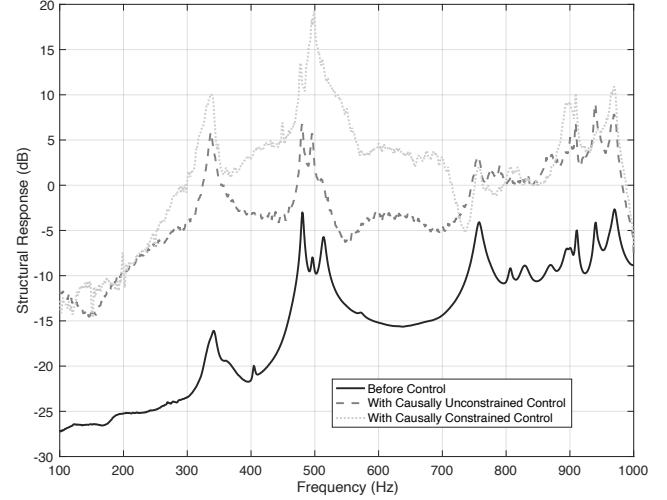
ing differences between the control efforts in each case, as shown in Figure 11.

4.3. Limits Due to Number of Control Actuators

It has been shown in the previous sections that the structural actuator array is able to effectively reduce the scattering from the finite-sized cylinder and the limits due to the use of a practical reference signal and imposing causality on the controller have also been demonstrated. However, in most practical applications, it is beneficial for the active control system to be as lightweight and low-cost as possible. This can be achieved by minimising the number of control actuators required. For this reason, an investigation into the reliance of the implemented active structural acoustic cloaking system on the number of control actuators has been carried out. Although a similar study into the effect of the number of control actuators was carried out by Eggler et al [14], this previous study investigated a cylinder of infinite length via simulations. Therefore, it is of interest to investigate the influence of the number of structural control actuators for the experimental configuration presented here.

The performance of the active structural acoustic cloaking system in terms of the broadband average attenuation in the scattered sound power has been calculated for increasing numbers of actuators between 1 and 9. In each case, the optimal configuration of actuators was selected through an exhaustive search. Due to the computational complexity of an exhaustive search, only the performance of the causally unconstrained controller has been investigated; however, these results are expected to be consistent regardless of the causality of the controller. Figure 13 presents the scattered acoustic power over frequency before control and with the causally unconstrained controller for an increasing number of control
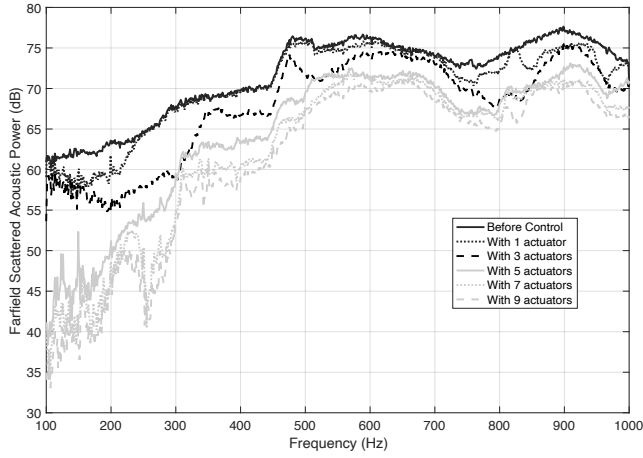
Figure 13: The scattered power before control, and with broadband unconstrained control with increasing numbers of control actuators.

Figure 14: The broadband attenuation within three frequency bands, for increasing numbers of control actuators

actuators. From these results it can be seen that with a single control actuator, reduction in the scattered acoustic pressure can only be achieved at frequencies below around 250 Hz. As the number of control actuators is increased, the control bandwidth also increases, and with 5 control actuators significant levels of control are achieved across the presented bandwidth. Increasing the number of control actuators further offers some additional improvements in the level of control achieved across the presented bandwidth, but the difference in performance between five, seven and nine actuators at frequencies above 500 Hz is less than 3 dB.

To provide further insight into the influence of the number of control actuators used, the performance presented in Figure 13 has been averaged over three frequency bands and the average broadband attenuation has been plotted against the number of control actuators in Figure 14. From these results it can be seen that, whilst the performance has not fully converged in any of the three frequency bands, it has reached a point where the increase in performance achieved by adding additional actuators is less than 1 dB. For example, increasing the number of actuators from 8 to 9 provides a broadband increase in performance of 0.7 dB, 0.8 dB and 0.3 dB in the three bandwidths respectively. It is interesting to note that to achieve a broadband average attenuation of around 6 dB requires 2 actuators up to 250 Hz, 4 actuators up to 500 Hz and 7 actuators up to 1 kHz, suggesting a doubling in bandwidth approximately requires a doubling in the number of control actuators.

5. Conclusions

This paper has investigated the limits on the performance of an active structural acoustic cloaking system using an experimental implementation with an aluminium cylindrical shell as the scattering body. An array of structural control sources was used to minimise the scattered acoustic pres-
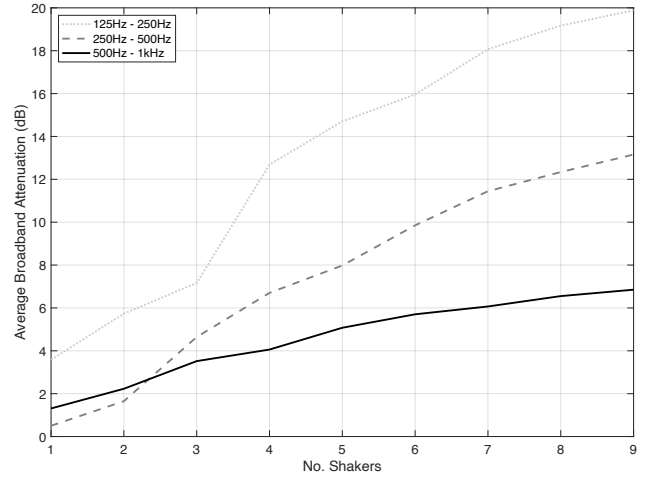
sure in the far-field using an optimal broadband feedforward control strategy, with a reference signal being provided via an IMC architecture. Using this configuration, it has been shown that at least 10 dB of attenuation in the far-field scattered acoustic power can be achieved across the bandwidth investigated. The impact of causally constraining the control filters was investigated, and it has been shown that the causality constraint required in broadband control systems limits the performance of the controller, particularly at low frequencies where the time-advance provided by the proposed reference signal is small compared to the period of oscillation. It has also been shown that the control effort required by the causally constrained controller is significantly greater than that required by the causally unconstrained controller and this can be related to a reduction in the efficiency of control. The effect of the active structural acoustic cloaking system on the structural response of the scattering structure has also been investigated for the first time, and it has been shown that the structural response is significantly enhanced. This may need to be considered in real-world applications, where an enhanced level of structural vibration may not be acceptable, even when it does not result in increased radiation. The influence of the number of control actuators on performance has also been investigated, and it has been shown how the number of structural control actuators required for successful acoustic cloaking increases as the bandwidth of control increases, with a doubling in control bandwidth approximately corresponding to a doubling in the number of required actuators.

The presented results provide new insight into the practicability of using structural actuation to minimise the acoustic scattering from an object. However, challenges to the realisation of fully practical active cloaking strategies that are capable of operating in non-stationary environments are still outstanding. For instance, the control strategy formulated in Section 3 assumes that the scattered pressure in the far-

field of the object is known, however, this limits practical realisations due to the reliance on a priori information and the resulting assumption of a stationary acoustic environment. To overcome this limitation, a practical active acoustic cloaking system, using either structural or acoustic control sources, would require a method of measuring or estimating the scattered acoustic pressure in real-time in non-stationary acoustic fields. Although a number of methods have been proposed in the literature for the real-time estimation of the scattered pressure, they also rely on a priori information that assumes a stationary acoustic environment and, therefore, further work is required in this area. In addition to the real-time measurement or estimation of the scattered acoustic pressure, it is necessary to obtain a real-time reference signal. In previous work, it was assumed that a reference signal was available directly from the primary source [10, 31, 38], which is often not practical. Therefore, in this paper, a reference signal has been calculated using an IMC architecture and the signal provided by a microphone located in the direction of the primary source. In a practical implementation, the direction of arrival of the incident wave may not be known, and therefore multiple reference microphones would need to be used to ensure that at least one reference signal is time-advanced compared to the scattered wave [45].

Acknowledgements

References

[1] L. Whitcomb, D. R. Yoerger, H. Singh, and J. Howland, "Advances in Underwater Robot Vehicles for Deep Ocean Exploration: Navigation, Control, and Survey Operations," *Robotics Research*, pp. 439–448, 2000.

[2] P. H. Fernandes, P. Stevenson, A. S. Brierley, F. Armstrong, and E. J. Simmonds, "Autonomous underwater vehicles: future platforms for fisheries acoustics," *ICES Journal of Marine Science*, vol. 60, no. 2, pp. 1–2, 2003.

[3] M. Long, *Architectural Acoustics*. Academic Press, 2nd edition ed., 2014.

[4] J. P. A. Lochner and J. F. Burger, "The influence of reflections on auditorium acoustics," *Journal of Sound and Vibration*, vol. 1, no. 4, pp. 426–448, 1964.

[5] J. B. Pendry, D. Schurig, and D. R. Smith, "Controlling electromagnetic fields.," *Science*, vol. 312, no. 5781, pp. 1780–1782, 2006.

[6] H. Chen and C. T. Chan, "Acoustic cloaking and transformation acoustics," *Journal of Physics D: Applied Physics*, vol. 43, no. 11, 2010.

[7] S. A. Cummer and D. Schurig, "One path to acoustic cloaking," *New Journal of Physics*, vol. 9, 2007.

[8] L. Zigoneanu, B. I. Popa, and S. A. Cummer, "Three-dimensional broadband omnidirectional acoustic ground cloak," *Nature Materials*, vol. 13, no. 4, pp. 352–355, 2014.

[9] P. A. Kerrian, A. D. Hanford, D. E. Capone, B. S. Beck, P. A. Kerrian, A. D. Hanford, D. E. Capone, and B. S. Beck, "Development of a perforated plate underwater acoustic ground cloak," *Journal of the Acoustical Society of America*, vol. 146, pp. 2303-2308, 2019.

[10] E. Friot and C. Bordier, "Real-time active suppression of scattered acoustic radiation," *Journal of Sound and Vibration*, vol. 278, no. 3, pp. 563–580, 2004.

[11] F. G. Vasquez, G. W. Milton, and D. Onofrei, "Broadband exterior cloaking," *Optical Society of America*, vol. 17, no. 17, pp. 568–571, 2009.

[12] A. N. Norris, F. A. Amirkulova, and W. J. Parnell, "Source amplitudes for active exterior cloaking," *Inverse Problems*, vol. 28, no. 10, 2012.

[13] G. Futhazar, W. J. Parnell, and A. N. Norris, "Active cloaking of flexural waves in thin plates," *Journal of Sound and Vibration*, vol. 356, pp. 1–19, 2015.

[14] D. Eggler, H. Chung, F. Montiel, J. Pan, and N. Kessissoglou, "Active noise cloaking of 2D cylindrical shells," *Wave Motion*, vol. 87, pp. 106–122, 2019.

[15] S. A. Cummer, J. Christensen, and A. Alù, "Controlling sound with acoustic metamaterials," *Nature Reviews Materials*, vol. 1, no. 16001, 2016.

[16] K. T. Tan, H. H. Huang, and C. T. Sun, "Optimizing the band gap of effective mass negativity in acoustic metamaterials," *Applied Physics Letters*, vol. 101, no. 24, 2012.

[17] J. Cheer, "Active control of scattered acoustic fields: Cancellation, reproduction and cloaking," *The Journal of the Acoustical Society of America*, vol. 140, no. 3, pp. 1502–1512, 2016.

[18] S. J. Elliott, *Signal Processing for Active Control*. Academic Press, 2001.

[19] P. A. Nelson and S. J. Elliott, *Active Control of Sound*. Academic Press, 1991.

[20] C. R. Fuller, S. J. Elliott, and P. A. Nelson, *Active Control of Vibration*. Academic Press, 1997.

[21] C. R. Fuller, C. H. Hansen, and S. Snyder, "Active control of sound radiation from a vibrating rectangular panel by sound sources and vibration inputs: An experimental comparison," *Journal of Sound and Vibration*, vol. 145, no. 2, 1991.

[22] B.-T. Wang, R. A. Burdisso, and C. R. Fuller, "Optimal Placement of Piezoelectric Actuators for Active Structural Acoustic Control," *Journal of Intelligent Material Systems and Structures*, vol. 5, no. 1, pp. 67–77, 1994.

[23] R. L. Clark and C. R. Fuller, "Active Control of Structurally Radiated Sound from an Enclosed Finite Cylinder," *Journal of Intelligent Material Systems and Structures*, vol. 5, no. 3, pp. 379–391, 1994.

[24] P. Gardonio and S. J. Elliott, "Smart panels for active structural acoustic control," *Smart Materials and Structures*, vol. 13, no. 6, pp. 1314–1336, 2004.

[25] J. Cheer and S. Daley, "Active structural acoustic control using the remote sensor method," *Journal of Physics: Conference Series*, vol. 744, no. 1, 2016.

[26] P. Aslani, S. D. Sommerfeldt, and J. D. Blotter, "Active control of simply supported cylindrical shells using the weighted sum of spatial gradients control metric," *The Journal of the Acoustical Society of America*, vol. 143, no. 1, pp. 271–280, 2018.

[27] J. Milton, J. Cheer, and S. Daley, "Experimental identification of the radiation resistance matrix," *The Journal of the Acoustical Society of America*, vol. 145, no. 5, pp. 2885–2894, 2019.

[28] M. Rajabi and A. Mojahed, "Active acoustic cloaking spherical shells," *Acta Acustica united with Acustica*, vol. 104, no. 1, pp. 5–12, 2018.

[29] E. G. Williams, *Fourier Acoustics - Sound Radiation and Nearfield Acoustical Holography*. Elsevier, 1999.

[30] C. House, J. Cheer, and S. Daley, "On the use of Virtual Sensing for the Real-Time Detection and Active Control of a Scattered Acoustic Field," in *International Congress on Sound & Vibration, Montreal July 2019*, no. 1, pp. 1–8, 2019.

[31] N. Han, X. Qiu, and S. Feng, "Active control of three-dimension impulsive scattered radiation based on a prediction method," *Mechanical Systems and Signal Processing*, vol. 30, pp. 267–273, 2012.

[32] F. G. Vasquez, G. W. Milton, and D. Onofrei, "Exterior cloaking with active sources in two dimensional acoustics," *Wave Motion*, vol. 48, no. 6, pp. 515–524, 2011.

[33] L. E. Kinsler and A. R. Frey, *Fundamentals of Acoustics*. John Wiley & Sons, 4th editio ed., 2000.

[34] Y. I. Bobrovnitskii, "A new solution to the problem of an acoustically

transparent body," *Acoustical Physics*, vol. 50, no. 6, pp. 647–650, 2004.

[35] Y. I. Bobrovnitskii, "A new impedance-based approach to analysis and control of sound scattering," *Journal of Sound and Vibration*, vol. 297, no. 3-5, pp. 743–760, 2006.

[36] Y. I. Bobrovnitskii, "Impedance acoustic cloaking," *New Journal of Physics*, vol. 12, pp. 0–20, 2010.

[37] C. Hansen and S. Snyder, *Active Control of Noise and Vibration*. CRC Press, 1st ed., 1996.

[38] E. Friot, R. Guillermin, and M. Winninger, "Active control of scattered acoustic radiation: A real-time implementation for a three-dimensional object," *Acta Acustica united with Acustica*, vol. 92, no. 2, pp. 278–288, 2006.

[39] M. Morai and E. Zafiriou, *Robust Process Control*. Prentice Hall, 1988.

[40] N. Abe, "Practical stability and disturbance rejection of internal model control for time-delay systems," *Proceedings of the IEEE Conference on Decision and Control*, vol. 2, no. December, pp. 1621–1622, 1996.

[41] L. Harnefors and H. P. Nee, "Model-based current control of ac machines using the internal model control method," *IEEE Transactions on Industry Applications*, vol. 34, no. 1, pp. 133–141, 1998.

[42] G. H. Golub, P. C. Hansen, and D. P. O'Leary, "Tikhonov Regularization and Total Least Squares," *Society for Industrial and Applied Mathematics Journal on Matrix Analysis and Applications*, 1999.

[43] M. Tohyama, *Sound & Signals*. Berlin: Springer-Verlag Berlin, 2011.

[44] C. House, J. Cheer, and S. Daley, "The Effect of Active Vibration Control on the Sound Field Scattered from a Flexible Structure," in *ISMA - International Conference on Noise and Vibration Engineering, Leuven September 2018*, (Leuven), 2018.

[45] J. Cheer, V. Patel, and S. Fontana, "The application of a multi-reference control strategy to noise cancelling headphones," *The Journal of the Acoustical Society of America*, vol. 145, no. 5, pp. 3095–3103, 2019.